# Study of Dalitz decay $\phi \rightarrow \eta e^+ e^-$ with KLOE detector

The KLOE-2 Collaboration

D. Babusci [h], I. Balwierz-Pytko [g], G. Bencivenni [h], C. Bloise [h],
F. Bossi [h], P. Branchini [r], A. Budano [q,r],
L. Caldeira Balkeståhl [u], F. Ceradini [q,r], P. Ciambrone [h],
F. Curciarello [i,d], E. Czerwiński [g], E. Danè [h], V. De Leo [i,d],
E. De Lucia [h], G. De Robertis [b], A. De Santis [h], P. De Simone [h],
A. Di Cicco [q,r], A. Di Domenico [m,n], R. Di Salvo [p],
D. Domenici [h], O. Erriquez [a,b], G. Fanizzi [a,b], A. Fantini [o,p],
G. Felici [h], S. Fiore [s,n], P. Franzini [m,n], A. Gajos [g], P. Gauzzi [m,n],
G. Giardina [i,d], S. Giovannella [h,*], E. Graziani [r], F. Happacher [h],
L. Heijkenskjöld [u] B. Höistad [u], T. Johansson [u], D. Kamińska [g],
W. Krzemien [g], A. Kupsc [u], J. Lee-Franzini [h,t], F. Loddo [b],
S. Loffredo [q,r], G. Mandaglio [i,d,c], M. Martemianov [j],
M. Martini [h,ℓ], M. Mascolo [o,p], R. Messi [o,p], S. Miscetti [h,*],
G. Morello [h], D. Moricciani [p], P. Moskal [g], A. Palladino [h],
A. Passeri [r], V. Patera [k,h], I. Prado Longhi [q,r], A. Ranieri [b],
P. Santangelo [h], I. Sarra [h,*], M. Schioppa [e,f], B. Sciascia [h],
M. Silarski [g], L. Tortora [r], G. Venanzoni [h], W. Wiślicki [v],
M. Wolke [u]

[a]*Dipartimento di Fisica dell'Università di Bari, Bari, Italy.*

[b]*INFN Sezione di Bari, Bari, Italy.*

[c]*Centro Siciliano di Fisica Nucleare e Struttura della Materia, Catania, Italy.*

[d]*INFN Sezione di Catania, Catania, Italy.*

[e]*Dipartimento di Fisica dell'Università della Calabria, Cosenza, Italy.*

[f]*INFN Gruppo collegato di Cosenza, Cosenza, Italy.*

[g]*Institute of Physics, Jagiellonian University, Cracow, Poland.*

[h]*Laboratori Nazionali di Frascati dell'INFN, Frascati, Italy.*

[i]*Dipartimento di Fisica e Scienze della Terra dell'Università di Messina, Messina, Italy.*

[j]*Institute for Theoretical and Experimental Physics (ITEP), Moscow, Russia.*

$^\mathrm{k}$*Dipartimento di Scienze di Base ed Applicate per l'Ingegneria dell'Università "La Sapienza", Roma, Italy.*

$^\ell$*Dipartimento di Scienze e Tecnologie applicate, Università "Guglielmo Marconi", Roma, Italy.*

$^\mathrm{m}$*Dipartimento di Fisica dell'Università "La Sapienza", Roma, Italy.*

$^\mathrm{n}$*INFN Sezione di Roma, Roma, Italy.*

$^\mathrm{o}$*Dipartimento di Fisica dell'Università "Tor Vergata", Roma, Italy.*

$^\mathrm{p}$*INFN Sezione di Roma Tor Vergata, Roma, Italy.*

$^\mathrm{q}$*Dipartimento di Matematica e Fisica dell'Università "Roma Tre", Roma, Italy.*

$^\mathrm{r}$*INFN Sezione di Roma Tre, Roma, Italy.*

$^\mathrm{s}$*ENEA UTTMAT-IRR, Casaccia R.C., Roma, Italy*

$^\mathrm{t}$*Physics Department, State University of New York at Stony Brook, USA.*

$^\mathrm{u}$*Department of Physics and Astronomy, Uppsala University, Uppsala, Sweden.*

$^\mathrm{v}$*National Centre for Nuclear Research, Warsaw, Poland.*

**Abstract**

We have studied the vector to pseudoscalar conversion decay $\phi \to \eta e^+ e^-$, with $\eta \to \pi^0 \pi^0 \pi^0$, with the KLOE detector at DA$\Phi$NE. The data set of 1.7 fb$^{-1}$ of $e^+ e^-$ collisions at $\sqrt{s} \sim \mathrm{M}_\phi$ contains a clear conversion decay signal of $\sim 31,000$ events from which we measured a value of $\mathrm{BR}(\phi \to \eta e^+ e^-) = (1.075 \pm 0.007 \pm 0.038) \times 10^{-4}$. The same sample is used to determine the transition form factor by a fit to the $e^+ e^-$ invariant mass spectrum, obtaining $\mathrm{b}_{\phi\eta} = (1.17 \pm 0.10^{+0.07}_{-0.11})\,\mathrm{GeV}^{-2}$, that improves by a factor of five the precision of the previous measurement and is in good agreement with VMD expectations.

*Key words:* $e^+ e^-$ Collisions, Conversion Decay, Transition Form Factor
*PACS:* 13.66.Bc, 13.40.Gp

## 1 Introduction

We report the study of the vector to pseudoscalar conversion decay $\phi \to \eta e^+ e^-$ with $\eta \to \pi^0 \pi^0 \pi^0$. In conversion decays, $A \to B\gamma^* \to B\,e^+ e^-$, the radiated

* Corresponding author.
  *Email addresses:* `simona.giovannella@lnf.infn.it` (S. Giovannella), `stefano.miscetti@lnf.infn.it` (S. Miscetti), `ivano.sarra@lnf.infn.it` (I. Sarra).

photon is virtual and the squared dilepton invariant mass, $M_{ee}^2$, corresponds to the photon 4-momentum transferred, $q^2$. The probability of having a lepton pair of given invariant mass is determined by the electromagnetic dynamical structure of the transition $A \to B\gamma^*$. The differential decay rate, normalized to the radiative width, is [1]:

$$\frac{1}{\Gamma(\phi \to \eta\gamma)}\frac{d\Gamma(\phi \to \eta\, e^+ e^-)}{dq^2} =$$
$$\frac{\alpha}{3\pi}\frac{|F_{\phi\eta}(q^2)|^2}{q^2}\sqrt{1 - \frac{4M^2}{q^2}}\left(1 + \frac{2M^2}{q^2}\right)\left[\left(1 + \frac{q^2}{M_\phi^2 - M_\eta^2}\right)^2 - \frac{4M_\phi^2 q^2}{(M_\phi^2 - M_\eta^2)^2}\right]^{3/2},$$

where $m$ is the mass of the electron and $M_\phi$, $M_\eta$ are the masses of the $\phi$ and $\eta$ mesons, respectively. $F_{\phi\eta}(q^2)$ is the transition form factor, TFF, that describes the coupling of the mesons to virtual photons and provides information on its nature and underlying structure. The slope of the transition form factor, $b_{\phi\eta}$, is defined as:

$$b_{\phi\eta} \equiv \frac{dF}{dq^2}\Big|_{q^2=0}. \tag{1}$$

In the Vector Meson Dominance model, VMD, the transition form factor is parametrized as:

$$F_{\phi\eta}(q^2) = \frac{1}{1 - q^2/\Lambda_{\phi\eta}^2} \quad \to \quad b_{\phi\eta} \approx \Lambda_{\phi\eta}^{-2}. \tag{2}$$

The VMD successfully describes some transitions, such as $\eta \to \gamma\mu^+\mu^-$, while is failing for others, as in the case of $\omega \to \pi^0\mu^+\mu^-$ [2]. Recently, new models have been developed to overcome such a kind of discrepancies [3,4] and they should be validated with the experimental data from other channels. The only existing data on $\phi \to \eta e^+e^-$ come from the SND [5] and CMD-2 [6] experiments. Their measurements of the branching ratio, BR($\phi \to \eta e^+e^-$), are $(1.19\pm0.19\pm0.07)\times10^{-4}$ and $(1.14\pm0.10\pm0.06)\times10^{-4}$, respectively. The VMD expectation is BR($\phi \to \eta e^+e^-$) $= 1.1\times10^{-4}$ [7]. The SND experiment has also measured the slope of the transition form factor from the $M_{ee}$ invariant mass distribution, on the basis of 213 events: $b_{\phi\eta}= (3.8\pm1.8)$ GeV$^{-2}$ [5]. The VMD expectation is $b_{\phi\eta}=1$ GeV$^{-2}$ [7].

Due to the large data sample, we have performed three different measurements:

(1) the determination of the branching fraction of the $\phi \to \eta e^+e^-$ decay;
(2) the direct measurement of the transition form factor slope $b_{\phi\eta}$ with a fit to the dilepton invariant mass spectrum;
(3) the extraction of the $|F_{\phi\eta}|^2$ as a function of the dilepton invariant mass.

## 2　The KLOE detector

DAΦNE , the Frascati $\phi$-factory, is an $e^+e^-$ collider running at center of mass energy of $\sim 1020$ MeV. Positron and electron beams collide at an angle of $\pi$-25 mrad, producing $\phi$ mesons nearly at rest. The KLOE experiment operated at this collider from 2000 to 2006, collecting 2.5 fb$^{-1}$. The KLOE apparatus consists of a large cylindrical Drift Chamber surrounded by a lead-scintillating fiber electromagnetic calorimeter both inserted inside a superconducting coil, providing a 0.52 T axial field. The beam pipe at the interaction region is a sphere with 10 cm radius, made of a 0.5 mm thick Beryllium-Aluminum alloy. The drift chamber [8], 4 m in diameter and 3.3 m long, has 12,582 all-stereo tungsten sense wires and 37,746 aluminum field wires, with a shell made of carbon fiber-epoxy composite with an internal wall of $\sim 1$ mm thickness. The gas used is a 90% helium, 10% isobutane mixture. The momentum resolution is $\sigma(p_\perp)/p_\perp \approx 0.4\%$. Vertices are reconstructed with a spatial resolution of $\sim$ 3 mm. The calorimeter [9], with a readout granularity of $\sim (4.4 \times 4.4)$ cm$^2$, for a total of 2440 cells arranged in five layers, covers 98% of the solid angle. Each cell is read out at both ends by photomultipliers, both in amplitude and time. The energy deposits are obtained from the signal amplitude while the arrival times and the particles positions are obtained from the time differences. Cells close in time and space are grouped into energy clusters. Energy and time resolutions are $\sigma_E/E = 5.7\%/\sqrt{E \text{ (GeV)}}$ and $\sigma_t = 57 \text{ ps}/\sqrt{E \text{ (GeV)}} \oplus 100$ ps, respectively. The trigger [10] uses both calorimeter and chamber information. In this analysis the events are selected by the calorimeter trigger, requiring two energy deposits with $E > 50$ MeV for the barrel and $E > 150$ MeV for the endcaps.

Machine parameters are measured online by means of large angle Bhabha scattering events. The average value of the center of mass energy is evaluated with a precision of about 30 keV each 200 nb$^{-1}$ of integrated luminosity. Collected data are processed by an event classification algorithm [11], which streams various categories of events in different output files.

## 3　Branching Ratio

The analysis of the decay chain $\phi \to \eta e^+e^-$, $\eta \to 3\pi^0$, has been performed on a data sample of about 1.7 fb$^{-1}$. The Monte Carlo (MC) simulation for the signal has been produced with $d\Gamma(\phi \to \eta e^+e^-)/dM_{ee}$ according to VMD model. The signal production corresponds to an integrated luminosity one hundred times larger than collected data. Final state radiation has been included using PHOTOS Monte Carlo generator [12]. For the background, all $\phi$ decays and the not resonant $e^+e^- \to \omega\pi^0$ process have been simulated with a statistics
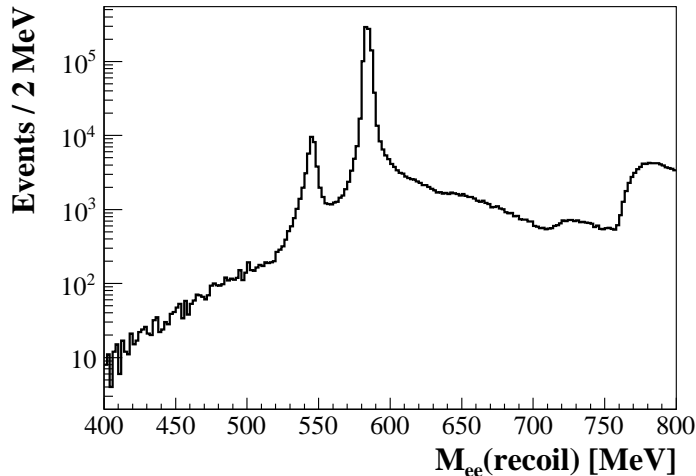
Fig. 1. Recoil mass against the $e^+e^-$ pair for the data sample after preselection cuts. The first peak on the left corresponds to the $\eta$ mass. The second peak at $\sim 590$ MeV is due to $K_S \to \pi^+\pi^-$ events with a wrong mass assignment.

two times larger than data.

All MC productions take into account changes in DAΦNE operation and background conditions on a run-by-run basis. Data-MC corrections for cluster energies and tracking efficiencies are evaluated with radiative Bhabha and $\phi \to \rho\pi$ samples, respectively. The main steps of the analysis are:

(1) a preselection requiring two tracks of opposite sign extrapolated to a cylinder around the interaction point and 6 prompt photon candidates;
(2) a loose cut on the six photon invariant mass: $400 < M_{6\gamma} < 700$ MeV;
(3) a $3\sigma$ cut on the recoil mass against the $e^+e^-$ pair, $M_{ee}(recoil)$, shown in Fig. 1: $536.5 < M_{ee}(recoil) < 554.5$ MeV [1];
(4) a cut on the invariant mass and the distance between the two tracks extrapolated to the beam pipe and at the drift chamber wall surfaces, to reject photon conversion;
(5) a cut based on the time of flight (TOF) of the tracks to the calorimeter to reject events with charged pions in the final state.

These cuts are described in details in ref. [13], which reports the results for a search of a light vector boson using the same data sample. The $M_{ee}$ and $\cos\psi^*$ [2] distributions, after the $M_{ee}(recoil)$ cut and at the end of the analysis chain, are shown in Fig. 2, compared to MC expectations. The residual

[1] We observed a shift of about 2 MeV with respect to the $\eta$ mass ($\sim 547.85$ MeV). The shift is due to the treatment of the energy loss for the electrons in the tracking reconstruction, that assumes the energy loss for pions.
[2] The $\cos\psi^*$ variable is defined as the angle between the $\eta$ and the $e^+$ in the $e^+e^-$ rest frame.
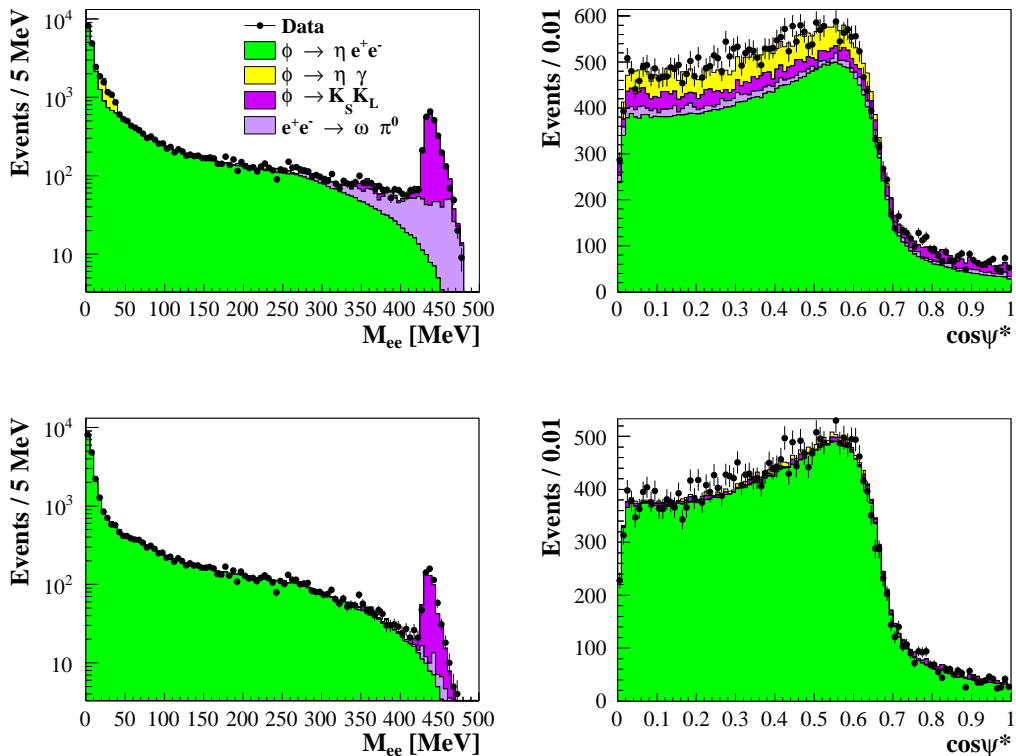
Fig. 2. Data-MC comparison for $M_{ee}$ (left) and $\cos\psi^*$ (right) distributions after the $M_{ee}(\text{recoil})$ cut (top) and at the end of the analysis chain (bottom). The signal production corresponds to an integrated luminosity one hundred times larger than collected data.

background contamination is concentrated at high masses and is dominated by $\phi \to K_S K_L \to \pi^+\pi^- 3\pi^0$ events with an early $K_L$ decay.

The analysis efficiency for signal events as a function of the $e^+e^-$ invariant mass is shown in Fig. 3 for 5 MeV mass bins. It is about 10% at low masses and increases to $\sim 35\%$ at 460 MeV, due to the larger acceptance for higher momentum tracks.

At the end of the analysis chain, 30,577 events are selected, with $\sim 3\%$ background contamination. After bin to bin background subtraction, $29,625\pm178$ $\phi \to \eta e^+e^-$, $\eta \to 3\pi^0$, candidates are present in the dataset.

The branching ratio has been calculated using bin-by-bin efficiency correction:

$$BR(\phi \to \eta e^+e^-) = \frac{\sum_i N_i/\epsilon_i}{\sigma_\phi \times \mathcal{L} \times BR(\eta \to 3\pi^0)}. \tag{3}$$

The luminosity measurement is obtained using very large angle Bhabha scattering events [14], giving an integrated luminosity of $\mathcal{L} = (1.68 \pm 0.01)$ fb$^{-1}$. The effective $\phi$ production cross section takes into account the center of mass
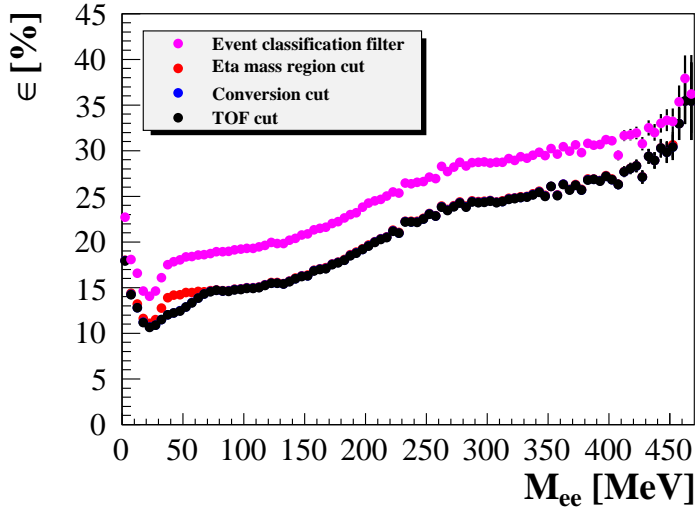
Fig. 3. Analysis efficiency as a function of $e^+e^-$ invariant mass for different steps of the selection procedure.

Table 1

Systematics on the branching ratio. Relative variation of each contribution with respect to the $M_{ee}$(recoil), TOF, Photon Conversion, Event Classification cuts are reported.

| CUT | | BR Variation |
|---|---|---|
| $M_{ee}$(recoil) | $\pm 1\sigma$ | (-0.1/+0.06)% |
| TOF | $\pm 1\sigma$ | (+0.01/-0.1)% |
| Photon conversion | $\pm 20\%$ | (-0.1/+0.1)% |
| Event Classification | $M_{ee} > 100\,\text{MeV}$ | -0.1% |
| | **Total** | **(-0.2/0.6)%** |

energy variations (at 1% level) [15]: $\sigma = (3310 \pm 120)$ nb. The value of the BR($\eta \to 3\pi^0$)=(32.57±0.23)% is taken from [16]. Our result is:

$$BR(\phi \to \eta e^+ e^-) = (1.075 \pm 0.007 \pm 0.038) \times 10^{-4}, \tag{4}$$

where the error includes the uncertainties on luminosity and $\phi$ production cross section. The systematic error has been evaluated moving by $\pm 1\sigma$ the analysis cuts on the recoil mass and TOF, and by $\pm 20\%$ those related to conversion cuts (Table 1). In order to evaluate the systematic due to the variation of the analysis efficiency for low $M_{ee}$ values, the BR has been measured for $M_{ee} > 100$ MeV, where the efficiency has a smoother behaviour. These systematics are negligible with respect to the normalization error.

7

## 4 Measurement of the electromagnetic transition form factor

The fit procedure, based on the MINUIT package [17], is applied to the $M_{ee}$ distribution, after a bin-by-bin background subtraction. Analysis efficiency and smearing effects have been folded into the theoretical function of Eq. 1, using as free parameters $\Lambda_{\phi\eta}$ with an overall normalization factor. The $M_{ee}$ distribution is then fitted, in the whole range, using a bin width of 5 MeV, by minimizing a $\chi^2$ function, defined as:

$$\chi^2 = \sum_{i=1}^{N} \frac{(N_{DATA}^i - N_{expected}^i)^2}{\sigma_i^2},$$ (5)

where $N_{DATA}$ is the number of event in the reconstructed i-th $M_{ee}$ bin after background subtraction and $N_{expected}$ is the expected number of events in the same bin, evaluated by performing a convolution of the theoretical function with reconstruction effects as follows:

$$N_{expected}^i = \sum_{j=1}^{N} f_{theor.}(m_j) \cdot p(M_{ee}^j, M_{ee}^i) \cdot \epsilon_j,$$ (6)

where $f_{theor.}(m_j)$ is the integrated VMD spectrum in the j-th bin, $p(m_{ee}^j, m_{ee}^i)$ is the probability for an events generated with mass $m_j$ to be reconstructed in the i-th bin and $\epsilon_j$ is the reconstruction efficiency in the j-th bin. The probability $p(m_{ee}^j, m_{ee}^i)$ is shown in Fig. 4. Smearing effects are of the order of few %. The resolution on the $M_{ee}$ variable has been evaluated for each mass bin applying a gaussian fit on the $M_{ee}(\text{rec.}) - M_{ee}(\text{true})$ and it is at the 2% level.

As result of the fit procedure, we determine a value of the form factor slope $b_{\phi\eta} = (1.17 \pm 0.10)$ GeV$^{-2}$, with $\chi^2/\text{ndf} = 1.17$ and a $\chi^2$ probability of about 13%. In Fig. 5 (top) the fit result is shown and compared with data. Fit normalized residuals, defined as $(N_{DATA}^i - N_{expected}^i)/\sigma_i$, are shown in Fig. 5 bottom left: the distribution of their values has the correct gaussian behaviour, centered at 0 with $\sigma = 1$ (Fig. 5 bottom right).
Systematics for the $M_{ee}(\text{recoil})$, TOF and photon conversion cuts have been evaluated as for the BR measurement and summarised in Table 2. Systematics related to the fit procedure have been evaluated as the RMS of the deviation from the central value obtained by varying the mass range used for the fit. The total systematic error is the quadrature of all contributions.
The result for the slope of the transition form factor is:

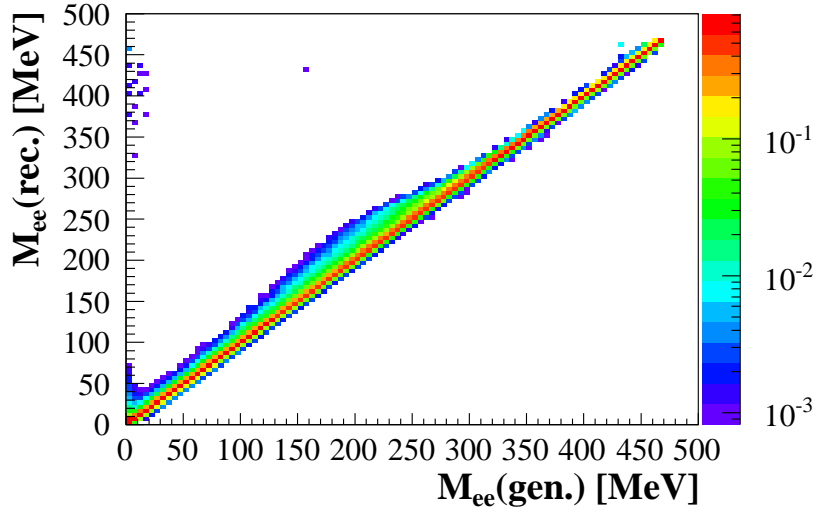$$b_{\phi\eta} = (1.17 \pm 0.10^{+0.07}_{-0.11}) \text{ GeV}^{-2}.$$ (7)

Fig. 4. Smearing matrix: reconstructed vs generated $M_{ee}$ values for $\phi \to \eta e^+ e^-$ MC events.

Table 2

Systematics on $b_{\phi\eta}$. Relative variation of each contribution with respect to the $M_{ee}$(recoil), TOF, Photon Conversion, Fit mass range cuts are reported.

| CUT | | $b_{\phi\eta}$ Variation |
|---|---|---|
| $M_{ee}$(recoil) | $\pm1\sigma$ | (+3.3/-4.6)% |
| TOF | $\pm1\sigma$ | (-2.5/1.5)% |
| Photon conversion | $\pm20\%$ | (-5.9/1.7)% |
| Fit Limits | $M_{ee}$ fit range | $\pm4.4\%$ |
| | Total | (-9.0/+6.0)% |

## 5    Transition form factor as a function of $M_{ee}$

The modulus squared of the transition form factor, $|F_{\phi\eta}(q^2)|^2$, as a function of the $e^+e^-$ invariant mass, is obtained by dividing bin by bin the $M_{ee}$ spectrum of Fig. 5 (top) by the one of reconstructed signal events, generated with $F_{\phi\eta}^{MC} = 1$, after all analysis cuts. MC sample is normalized in order to reproduce the number of events in the first bin of data. In Table 3, the values of $|F_{\phi\eta}(q^2)|^2$ as a function of the dilepton invariant mass, with the corresponding statistical errors are reported.

The $|F_{\phi\eta}(q^2)|^2$ distribution has been fitted as a function of the invariant mass with two free parameters, one corresponding to the normalization and the other to $\Lambda_{\phi\eta}$, as shown in Fig. 6, together with the predictions form the VMD
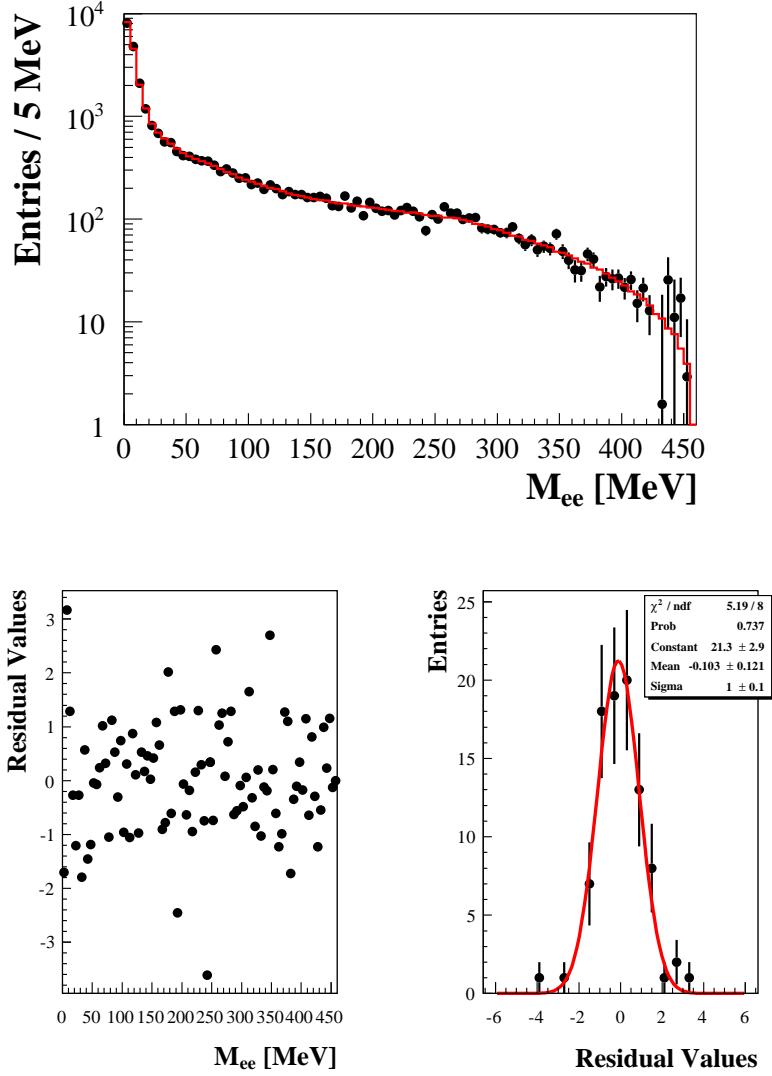
9

Fig. 5. Top: fit to the $M_{ee}$ spectrum for the Dalitz decays $\phi \rightarrow \eta\,e^+e^-$, with $\eta \rightarrow \pi^0\pi^0\pi^0$, in logarithmic scale. Bottom left: normalized fit residuals vs $M_{ee}$. Bottom right: distribution of normalized values with superimposed a gaussian fit.

and from ref. [3]. From this fit, the value of the slope $b_{\phi\eta}$ is:

$$b_{\phi\eta} = (1.25 \pm 0.10)\ \mathrm{GeV}^{-2}, \tag{8}$$

in agreement within the uncertainties with the value obtained from the fit to the invariant mass spectrum (Eq. 7).

10

Table 3
Transition form factor $|F_{\phi\eta}|^2$ of the $\phi \to \eta e^+ e^-$ decay.

| $M_{ee}$ (MeV) | $|F_{\phi\eta}|^2$ | $\delta|F_{\phi\eta}|^2$ | $M_{ee}$ (MeV) | $|F_{\phi\eta}|^2$ | $\delta|F_{\phi\eta}|^2$ | $M_{ee}$ (MeV) | $|F_{\phi\eta}|^2$ | $\delta|F_{\phi\eta}|^2$ |
|---|---|---|---|---|---|---|---|---|
| 2.50 | 1.00 | 0.01 | 157.50 | 1.17 | 0.09 | 312.50 | 1.57 | 0.17 |
| 7.50 | 1.05 | 0.02 | 162.50 | 1.13 | 0.09 | 317.50 | 1.28 | 0.16 |
| 12.50 | 1.03 | 0.02 | 167.50 | 0.98 | 0.08 | 322.50 | 1.19 | 0.16 |
| 17.50 | 0.99 | 0.03 | 172.50 | 1.03 | 0.09 | 327.50 | 1.38 | 0.18 |
| 22.50 | 0.97 | 0.04 | 177.50 | 1.28 | 0.10 | 332.50 | 1.21 | 0.18 |
| 27.50 | 1.00 | 0.04 | 182.50 | 1.03 | 0.09 | 337.50 | 1.35 | 0.19 |
| 32.50 | 0.93 | 0.04 | 187.50 | 1.21 | 0.10 | 342.50 | 1.39 | 0.20 |
| 37.50 | 1.03 | 0.05 | 192.50 | 0.90 | 0.09 | 347.50 | 2.08 | 0.26 |
| 42.50 | 0.95 | 0.05 | 197.50 | 1.25 | 0.10 | 352.50 | 1.50 | 0.25 |
| 47.50 | 0.95 | 0.05 | 202.50 | 1.12 | 0.10 | 357.50 | 1.30 | 0.24 |
| 52.50 | 1.01 | 0.05 | 207.50 | 1.05 | 0.10 | 362.50 | 1.13 | 0.28 |
| 57.50 | 1.01 | 0.05 | 212.50 | 1.13 | 0.10 | 367.50 | 1.20 | 0.27 |
| 62.50 | 1.03 | 0.05 | 217.50 | 1.04 | 0.10 | 372.50 | 1.87 | 0.29 |
| 67.50 | 1.08 | 0.06 | 222.50 | 1.14 | 0.10 | 377.50 | 1.76 | 0.29 |
| 72.50 | 1.04 | 0.06 | 227.50 | 1.27 | 0.11 | 382.50 | 1.02 | 0.29 |
| 77.50 | 0.96 | 0.06 | 232.50 | 1.18 | 0.11 | 387.50 | 1.49 | 0.31 |
| 82.50 | 1.09 | 0.06 | 237.50 | 1.06 | 0.10 | 392.50 | 1.58 | 0.36 |
| 87.50 | 1.06 | 0.06 | 242.50 | 0.83 | 0.10 | 397.50 | 1.79 | 0.38 |
| 92.50 | 1.01 | 0.06 | 247.50 | 1.20 | 0.11 | 402.50 | 1.54 | 0.37 |
| 97.50 | 1.08 | 0.07 | 252.50 | 1.11 | 0.11 | 407.50 | 2.08 | 0.43 |
| 102.50 | 0.98 | 0.07 | 257.50 | 1.52 | 0.13 | 412.50 | 1.40 | 0.48 |
| 107.50 | 1.06 | 0.07 | 262.50 | 1.33 | 0.12 | 417.50 | 2.24 | 0.59 |
| 112.50 | 0.97 | 0.07 | 267.50 | 1.39 | 0.13 | 422.50 | 1.40 | 0.59 |
| 117.50 | 1.12 | 0.08 | 272.50 | 1.24 | 0.13 | 427.50 | -0.14 | 1.36 |
| 122.50 | 1.05 | 0.08 | 277.50 | 1.32 | 0.13 | 432.50 | 0.28 | 3.02 |
| 127.50 | 0.96 | 0.07 | 282.50 | 1.39 | 0.14 | 437.50 | 5.36 | 3.59 |
| 132.50 | 1.09 | 0.08 | 287.50 | 1.18 | 0.13 | 442.50 | 2.75 | 3.68 |
| 137.50 | 1.06 | 0.08 | 292.50 | 1.20 | 0.13 | 447.50 | 6.97 | 4.10 |
| 142.50 | 1.08 | 0.08 | 297.50 | 1.27 | 0.14 | 452.50 | 1.44 | 3.79 |
| 147.50 | 1.06 | 0.08 | 302.50 | 1.22 | 0.14 | 457.50 | 3.43 | 4.91 |
| 152.50 | 1.11 | 0.09 | 307.50 | 1.30 | 0.15 | | | |

# 6   Conclusions

Analysing the $\phi \to \eta e^+ e^-$ decay channel, an precise measurements of both, the BR($\phi \to \eta e^+ e^-$), and the transition form factor slope $b_{\phi\eta}$ are obtained. We measured a value of BR($\phi \to \eta e^+ e^-$) $=(1.075 \pm 0.007 \pm 0.038) \times 10^{-4}$ and a value of the slope of $b_{\phi\eta} = (1.17 \pm 0.10^{+0.07}_{-0.11}) \, \text{GeV}^{-2}$.

The BR($\phi \to \eta e^+ e^-$) is in agreement with VMD predictions [7] and with the SND and CMD-2 results [5,6]. The transition form factor slope is in agreement with VMD predictions [7], with a precision that is a factor of five better than previous SND measurement.

The transition form factor has been used [18] to derive the upper limit for the production of a light dark boson U in $\phi \to \eta U \to \eta e^+ e^-$ decay. Present measurement confirms the exclusion plot obtained by KLOE in the mass range $(5 < M_U < 470)$ MeV, where $b_{\phi\eta} = 1 \, \text{GeV}^{-2}$ was assumed [13].
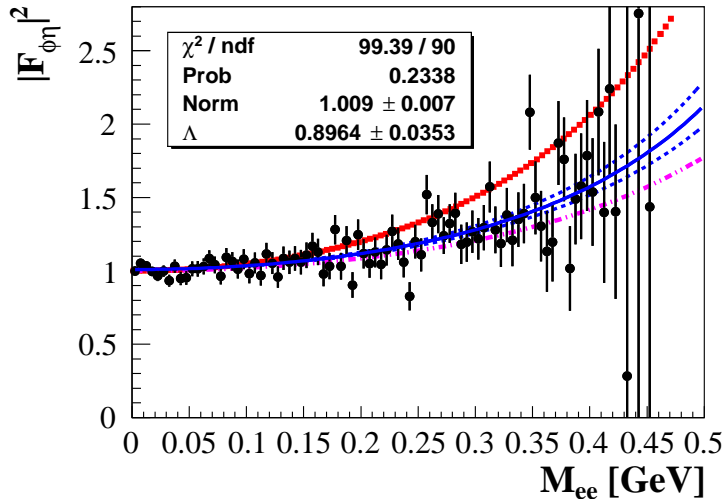
Fig. 6. Fit to the $|F_{\phi\eta}|^2$ distribution as a function of the invariant mass of the electron positron pair, with a binning of 5 MeV. The blue curve is the fit result, and in dashed blue the functions obtained for $\Lambda_{\phi\eta}=\Lambda_{\phi\eta} \pm 1\sigma$ are reported. VMD expectations are superimposed in pink while the curve obtained from reference [3] is reported in red.

## Acknowledgments

# References

[1]  L.G. Landsberg, Phys. Rep. 128, 301 (1985).

[2]  G. Usai, et al. [NA60 Collaboration], Nucl. Phys. A 855 189-196 (2011).

[3]  C. Terschlusen and S. Leupold, Phys. Lett. B 691, 191-201 (2010).

[4]  S. Ivashyn, Prob. Atomic Sci. Technol. 2012N1, 179-182 (2012).

[5]  M. N. Achasov et al. [SND collaboration], Phys. Lett. B 504, 275 (2001).

[6]  R.R. Akhmetshin et al. [CMD-2 collaboration], Phys. Lett. B 501,191 (2001).

[7]  A. Faessler, C. Fuchs, M. I. Krivoruchenko, Phys. Rev. C 61, 035206 (2000).

[8]  M. Adinolfi et al., Nucl. Inst. and Meth. A 488, 51 (2002).

[9]  M. Adinolfi et al., Nucl. Inst. and Meth. A 482, 364 (2002).

[10] M. Adinolfi et al., Nucl. Inst. and Meth. A 492, 134 (2002).

[11] F. Ambrosino et al., Nucl. Inst. and Meth. A 534, 403 (2004).

[12] E. Barberio and Z. Was, Comput. Phys. Commun. 79, 291-308 (1994).

[13] D. Babusci *et al.* [KLOE-2 Collaboration], Phys.Lett. B720 (2013) 111-115.

[14] F. Ambrosino et al. [KLOE collaboration], Eur. Phys. J C 47, 589-596 (2006).

[15] S. Giovannella, S. Miscetti, KLOE note 177 (2002).

[16] J. Beringer et al. [Particle Data Group], Phys. Rev. D 86, 010001 (2012).

[17] http://wwwasdoc.web.cern.ch/wwwasdoc/minuit/minuit.ps.

[18] M. Reece, L.T. Wang, JHEP 07, 051 (2009);